Supplementary Information

Theory of nonvolatile resistive switching in monolayer molybdenum disulfide with passive electrodes

Sanchali Mitra[†*], Arnab Kabiraj[†] and Santanu Mahapatra

Nano-Scale Device Research Laboratory, Department of Electronic Systems Engineering,

Indian Institute of Science (IISc), Bangalore 560012, India.

[†] These authors contributed equally.

* Corresponding author. Email: sanchalim@iisc.ac.in

Supplementary Table 1. Comparison of chemical properties of 2H-MoS_2 and $MoTe_2$.

Quantity	MoS_2	$MoTe_2$
Bader charge Mo (e)	1.08	0.48
Bader charge chalcogen (e)	-0.54	-0.24
DDEC charge Mo (e)	0.51	0.12
DDEC charge chalcogen (e)	-0.25	-0.06
DDEC total bond order Mo (e)	4.95	4.83
DDEC total bond order chalcogen (e)	2.82	3.25
$ICOHP_{Mo\text{-}chalcogen}$	-3.11	-2.39
$ICOHP_{Mo\text{-}Mo}$	-0.58	-0.42
$ICOHP_{chalcogen\text{-}chalcogen}$	-0.14	-0.24

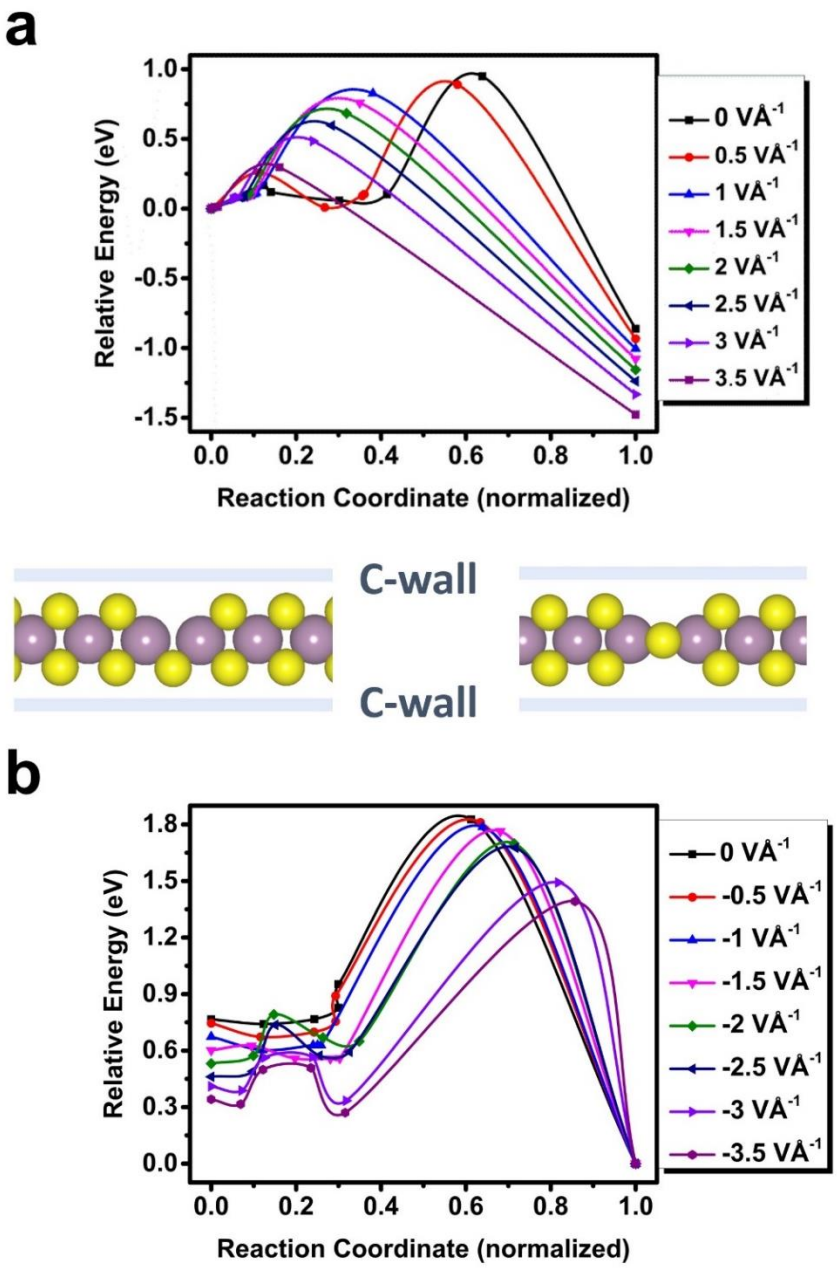

Supplementary Figure 1. CINEB calculations between S vacancy and popped state in MoS_2 monolayer placed between two implicit graphene walls. Electric field-dependent activation energy barriers for **a** S atom popping (forward reaction) and **b** return (reverse reaction). The atomistic picture of the initial and final states have been illustrated with Mo (purple balls) and S (yellow balls) atoms. Note that the energy in the y-axis is relative and only represents the barrier height and relative total energy difference between the two terminal points. Therefore, only the barriers under different electric fields can be compared from these plots, not the absolute values of total energies. The CINEB calculations have been done taking into account the potential energy contributions from the electric fields.

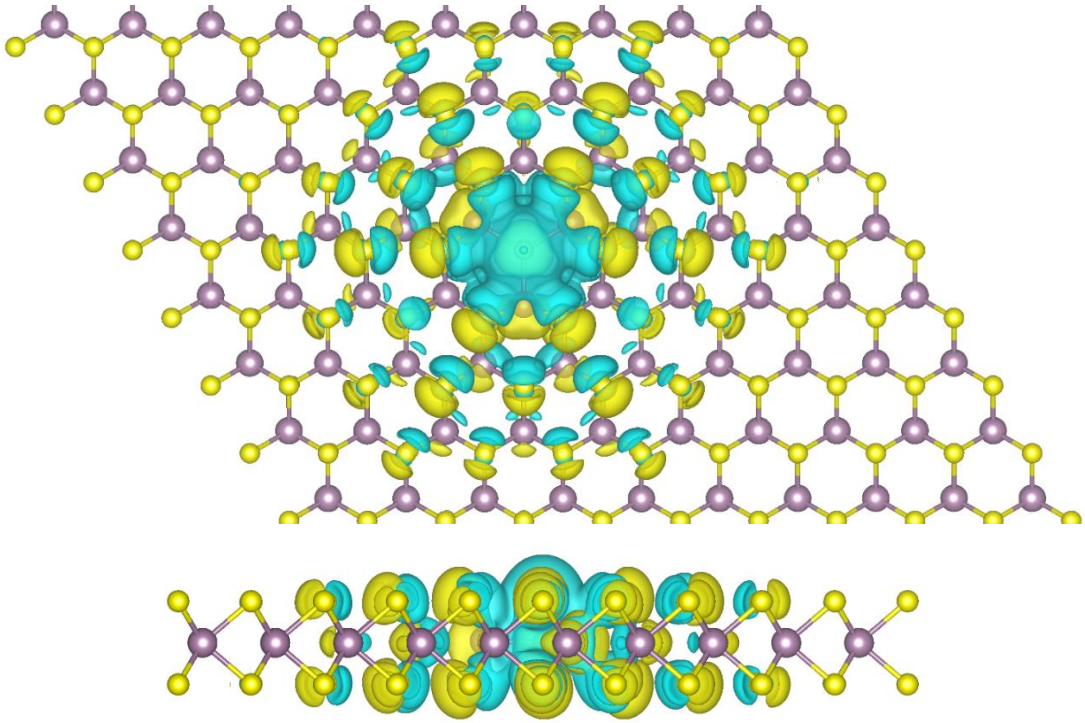

Supplementary Figure 2. Top and side views of charge density difference between the popped and parent-vacancy state. The popped atom is at the center of the cell. The blue clouds represent electron (negative charge) accumulation, while the yellow cloud represents electron depletion. The isosurface level is set at 0.006 eVÅ^{-3}.

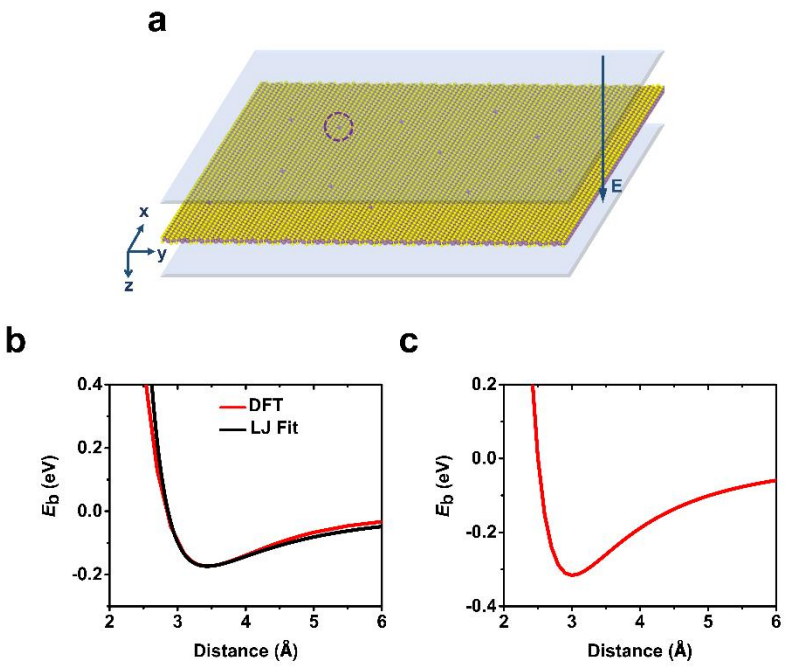

Supplementary Figure 3. MoS_2-LJ wall-based system and their interaction potential. **a** Atomic configuration of monolayer MoS_2 flake of dimension 18.9 nm × 26.5 nm comprising 12 scattered S monovacancies in the bottom S (lower *z*) plane. The transparent blue sheets represent two flat walls with Lennard Jones 9/3 potential to emulate C (/Au)-MoS_2 interactions. The direction of the electric field applied to set the device in the low resistance state is shown. The plot of binding energy vs. interlayer distance of **b** graphene-MoS_2 calculated using DFT and fitted with LJ 9/3 potential having energy and distance parameters $\varepsilon = 0.1646$ eV, $\sigma = 4.0$ Å, **c** Au-MoS_2 system with LJ 9/3 potential parameters $\varepsilon = 0.3$ eV and $\sigma = 3.5$ Å. See Supplementary Note 1 for more details.

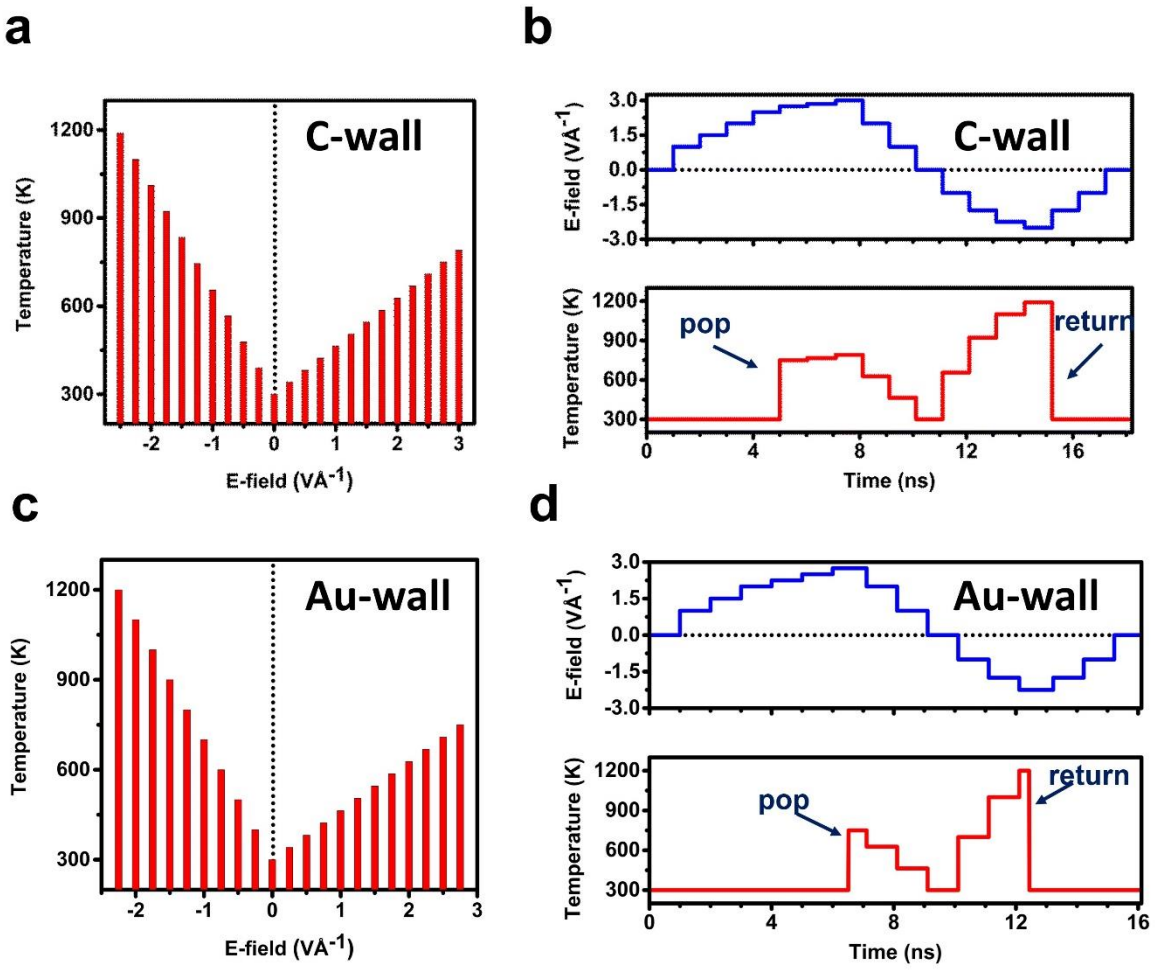

Supplementary Figure 4. Temperature mapping during MD simulations. The plot of assigned local temperatures vs. electric field for set and bipolar reset for **a** C(wall)-MoS_2-C(wall) and **c** Au(wall)-MoS_2-Au(wall) system. The rate of local temperature change for set is 164 $KV^{-1}Å$ for both C(wall) and Au(wall), while for reset is 355 $KV^{-1}Å$ for C wall and 400 $KV^{-1}Å$ for Au wall.

The plot of local temperature change of virtual filament regions during the entire set and reset cycle for **b** C wall and **d** Au wall-based systems. The top plot shows the applied electric field with simulation time, and the bottom plot depicts the local temperature change of a filament region with simulation time. Immediately after popping at 2.75 $VÅ^{-1}$, the local temperature around the popped atoms is ramped-up to 750K in 10 ps. Until reset, the temperature is varied according to the applied field, as depicted in plot **a**. As soon as return occurs at -2.25 $VÅ^{-1}$, the temperature around the returned atoms is ramped-down to 300K in 10ps.

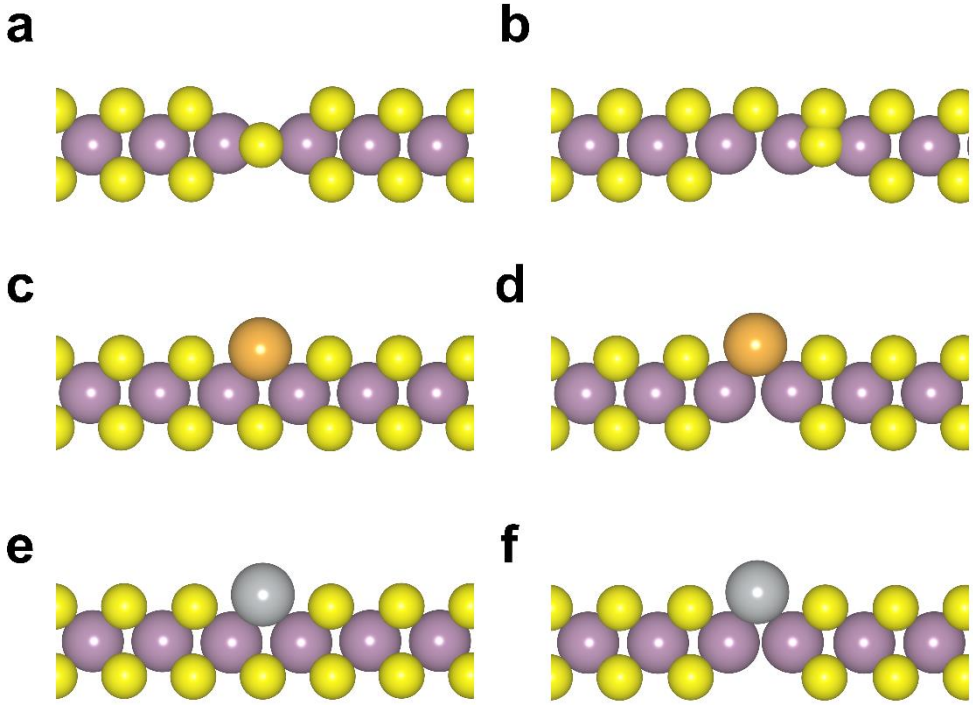

Supplementary Figure 5. Schematics of various events at vacancy site. Zoomed-in side view schematic of MoS_2 monolayer consisting of **a** primary popped atom, **b** secondary popped atom, Au absorbed in **c** S monovacancy, and **d** S divacancy, Ag absorbed in **e** S monovacancy and **f** S divacancy. The purple, yellow, golden, and silver balls represent Mo, S, Au, and Ag atoms**.**

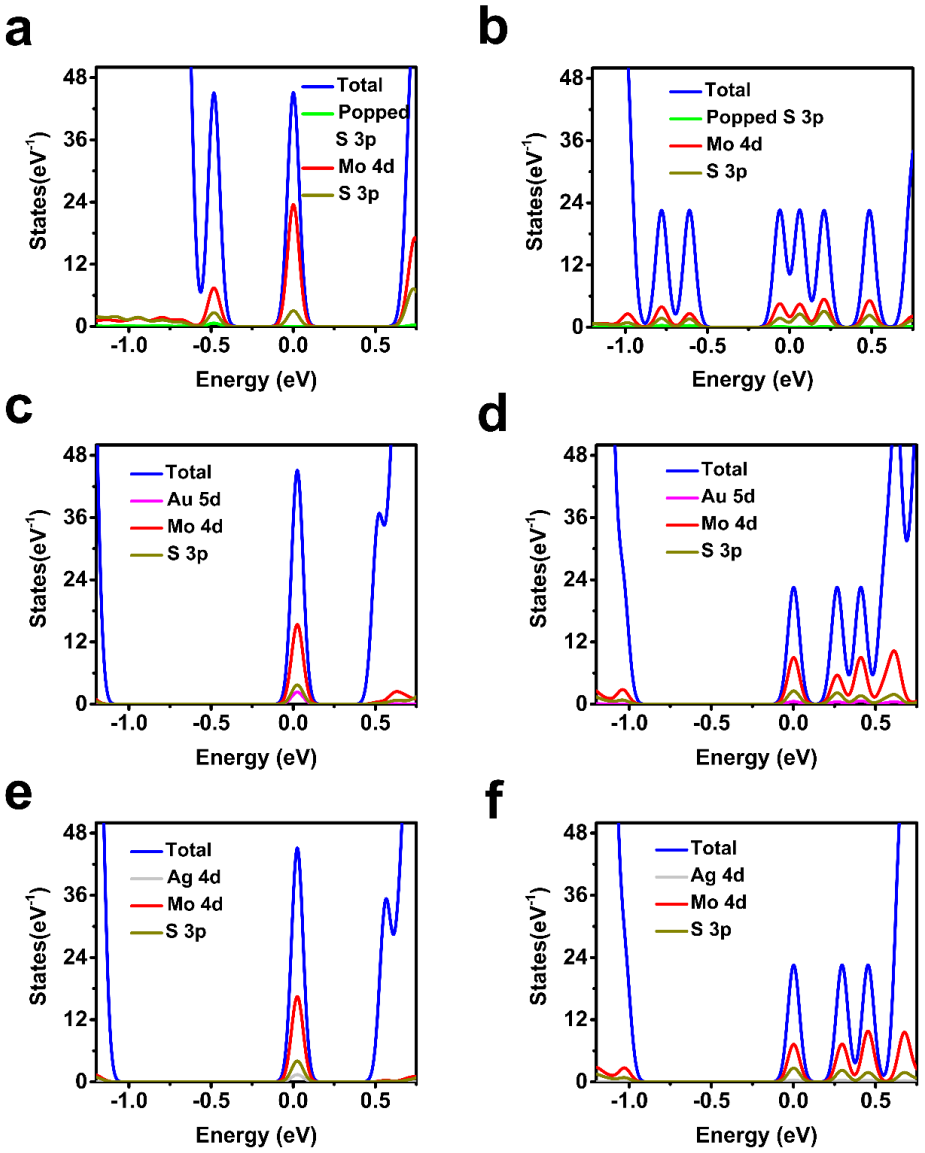

Supplementary Figure 6. DOS analyses. Calculated DOS of 10×10 supercell of monolayer MoS_2 consisting **a** popped S atom (Supplementary Fig. 3a), **b** secondary popped atom (Supplementary Fig. 3b), **c** Au absorbed in S monovacancy (Supplementary Fig. S3c), **d** Au absorbed in S divacancy (Supplementary Fig. 3d), **e** Ag absorbed in S monovacancy (Supplementary Fig. 3e), **f** Ag absorbed in S divacancy (Supplementary Fig. S3f). In addition to total DOS the contributions from popped atoms, absorbed Au/Ag atom, nearest 3 Mo atoms, and nearest 12 S atoms (13 for secondary pop and Au/Ag monovacancy) are shown.

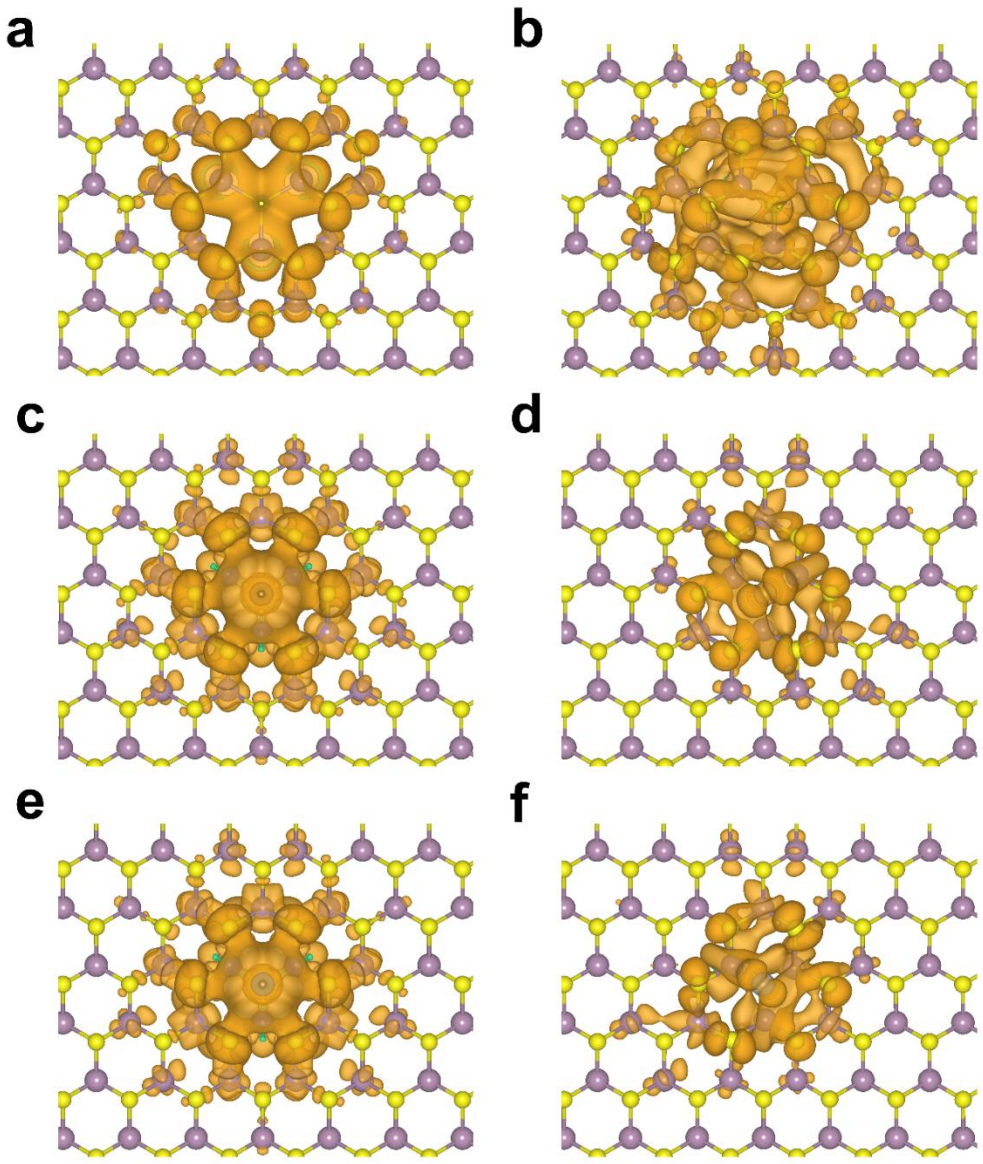

Supplementary Figure 7. Visualizing localized states. Energy-projected charge density isosurface plots for states very close to the Fermi level of **a** primary popped atom, **b** secondary popped atom, Au absorbed in **c** S monovacancy, and **d** S divacancy, Ag absorbed in **e** S monovacancy and **f** S divacancy. Evidently, conducting areas for the popped atoms and Au/Ag absorbed in the monovacancy sites are nearly equal, while the conducting region around Au/Ag atom absorbed in divacancy sites are slightly smaller. All isosurfaces are drawn for charge contributions to states in the energy range (-0.15, 0.15) eV, where the Fermi energy is defined as 0 eV. The isosurface levels are set as 0.005 eVÅ^{-3}.

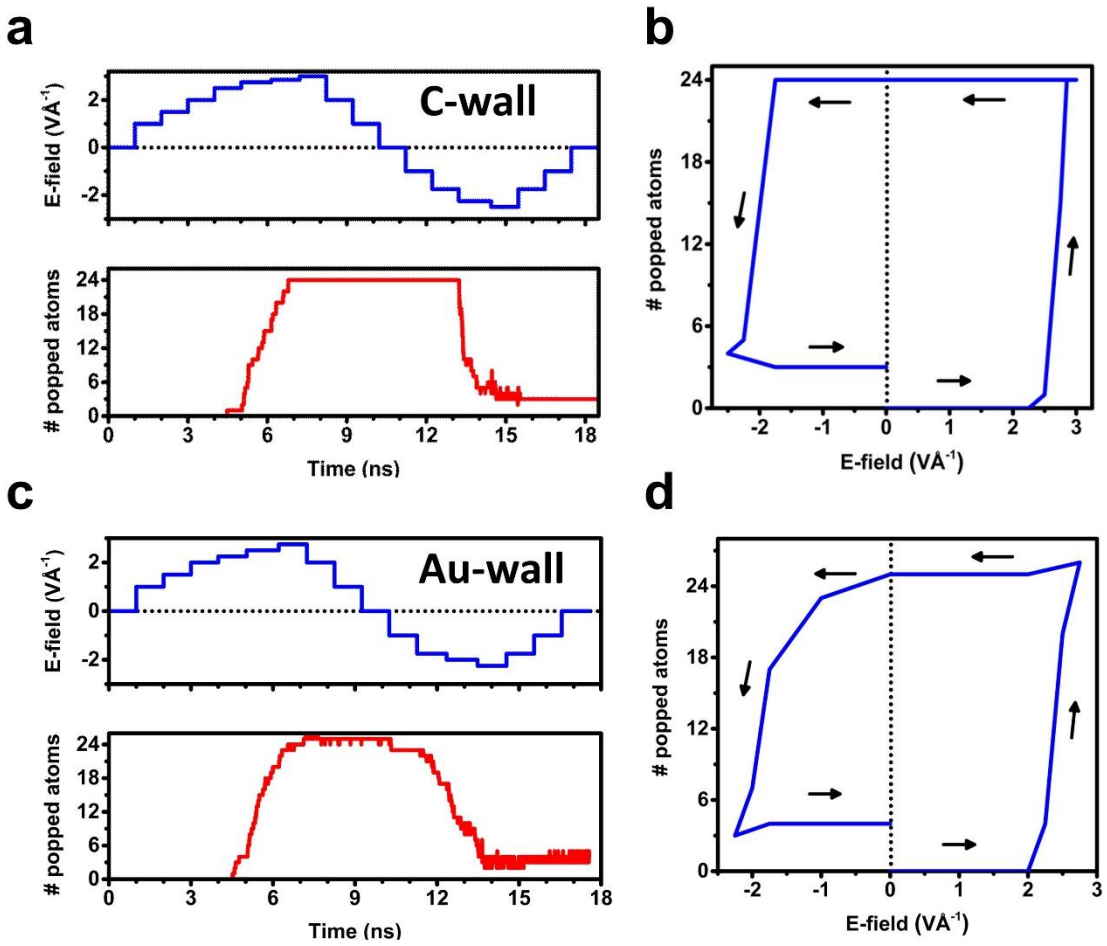

Supplementary Figure 8. Bipolar switching in monolayer MoS_2 consisting of 24 sulfur monovacancies (vacancy concentration 0.16%) in the bottom S plane. The plot of applied electric field and number of popped atoms vs. simulation time for **a** C(wall)-MoS_2-C(wall) and **c** Au(wall)-MoS_2-Au(wall) systems. Hysteresis plot showing the change in the pop count with the applied field for **b** C wall and **d** Au wall. For the C-MoS_2-C system, popping initiates at an applied field of 2.5 VÅ^{-1}, and after 2.85 VÅ^{-1}, the pop count increases to 24. The local temperatures have been varied using the same scheme illustrated in Supplementary Fig. 4. The return process starts at -2.25 VÅ^{-1}, and the pop count drops to 4, comprising only secondary pops. While returning to 0 VÅ^{-1}, one secondary popped atom returned to its initial location. For the Au-MoS_2-Au system, popping initiates at an applied field of 2.25 VÅ$^{-1,}$ and after 2.75 VÅ^{-1}, the pop count increases to 26, including 2 secondary pops. The return process is quite gradual. After a reverse field of -2.25 VÅ^{-1}, the pop count drops to 4.

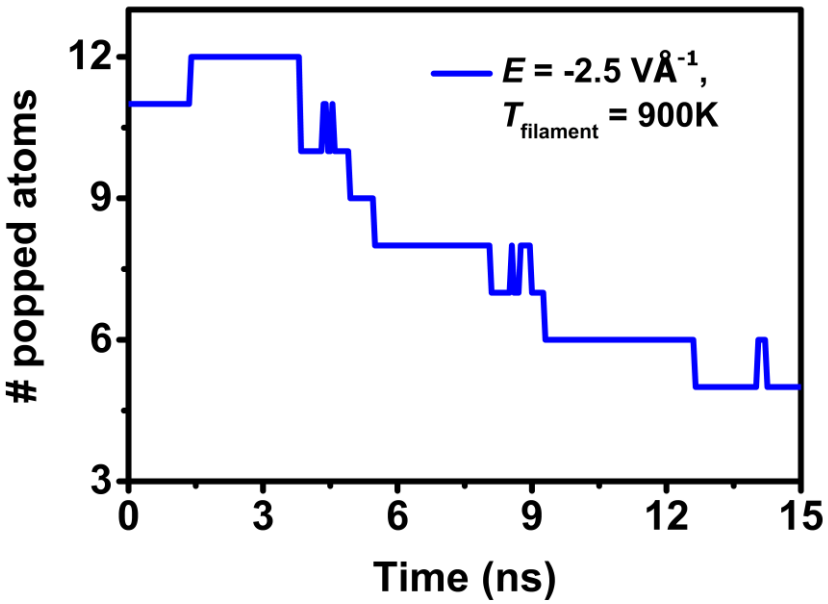

Supplementary Figure 9. Long time scale reset for Au(wall)-MoS_2-Au(wall). After the set cycle, a reverse field of -2.5 VÅ^{-1} is directly applied for 15 ns, and the local temperature around the popped atoms is raised to 900 K. The rate of filament temperature change is r_{reset} = 240 KV^{-1}Å, much lower than the initially assigned rate of 400 KV^{-1}Å. The return process is also quite slow, suggesting a long simulation is required to achieve switching at a lower temperature rate.

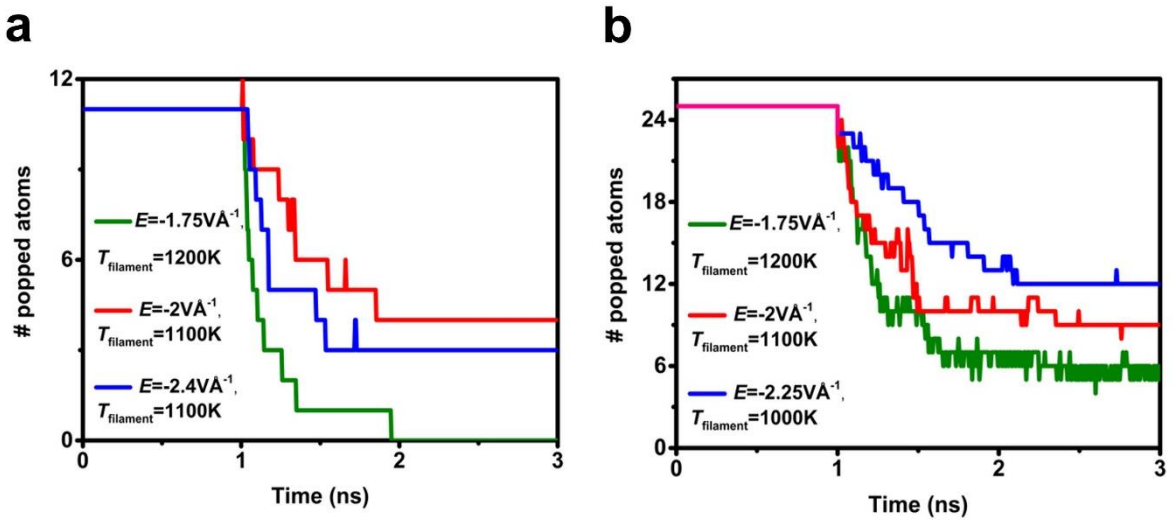

Supplementary Figure 10. Multilevel Switching characteristics. The plot of popped atom count with simulation time for **a** C(wall)-MoS_2-C(wall) sample consisting of 12 vacancies (0.08%) and **b** Au(wall)-MoS_2-Au(wall) consisting of 24 vacancies (0.16%). After the set cycle, three different electric fields of values -1.75, -2, -2.4 VÅ^{-1} for C-wall and -1.75, -2, -2.25 VÅ^{-1} for

Au-wall are applied. Correspondingly, local temperatures are raised to 1200, 1100, and 1100 K (1000K for Au-wall). The drop in the pop counts is different for different reset conditions, indicating the existence of multilevel resistance states as reported in Ref.[1,2]

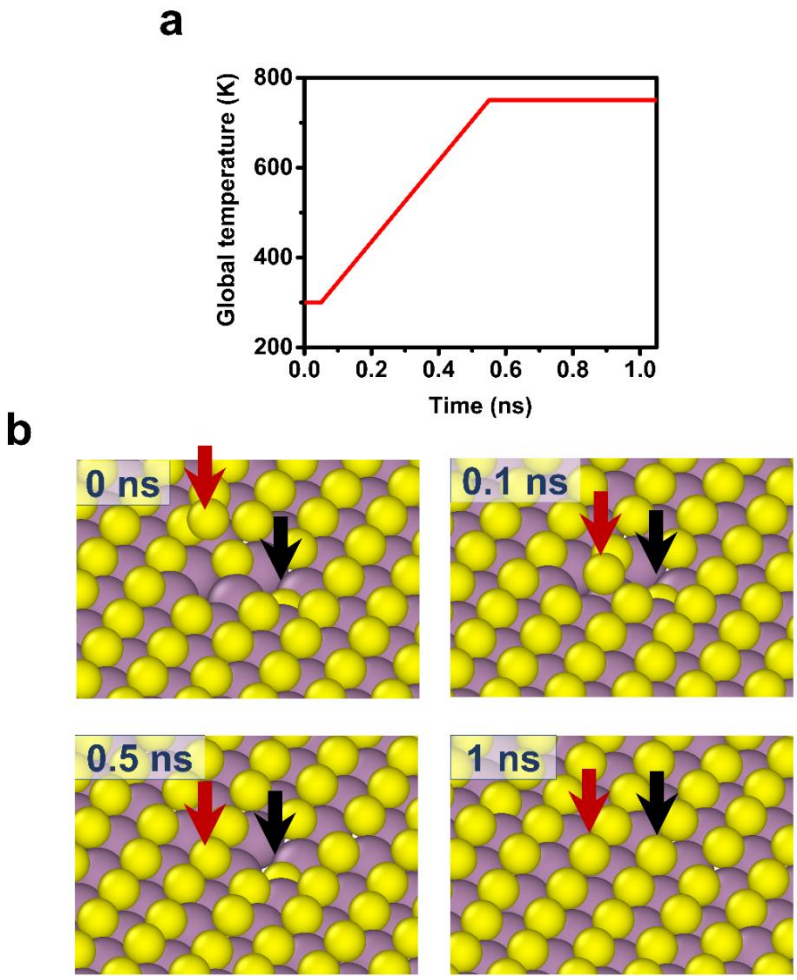

Supplementary Figure 11. Annealing of MoS_2 monolayer sample consisting of secondary popped S atoms generated during the reset process. During the simulation, S adatoms are placed close to the MoS_2 surface near the secondary popped atoms, and the global temperature of the system is increased. **a** The plot of global temperature change with simulation time. **b** Atomistic snapshots zooming-in at a secondary pop location at different points of time. The black arrow highlights the secondary popped atom, and the red arrow points to the S adatom. During heating from 300-750 K, the S adatom occupies the vacancy location, and at 750 K, the secondary popped S atom returns to its initial location. In the reset cycle, the generation of a large number of secondary popped atoms may hinder switching from low resistance to a high resistance state.

Annealing in an S-rich atmosphere may replace some of the vacancies with extra S atoms, triggering the return of popped atoms.[3]

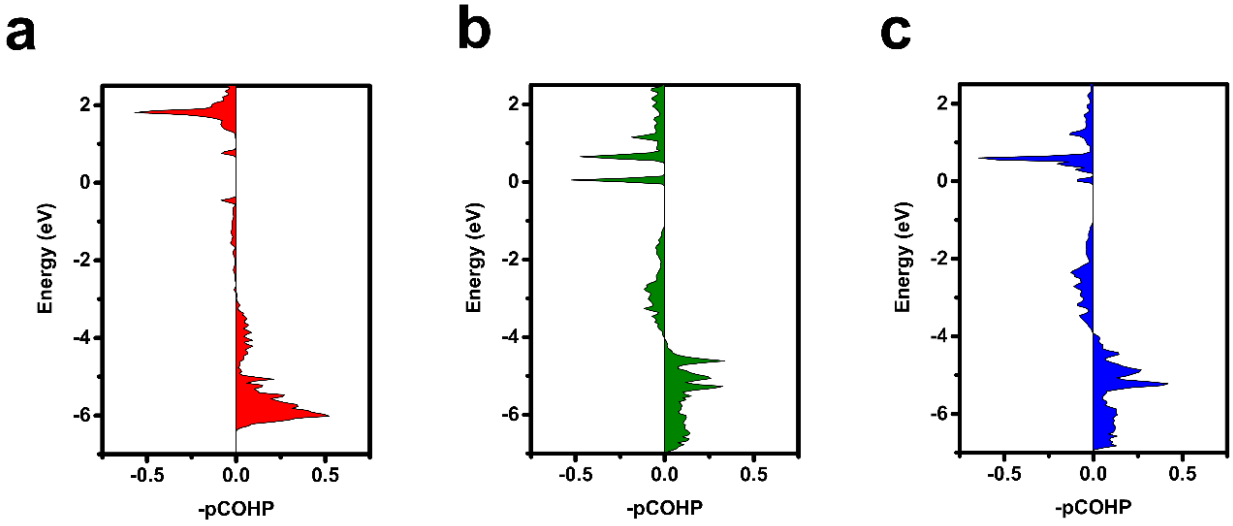

Supplementary Figure 12. COHP plots. The plots for **a** S popped, **b** Au absorbed in S monovacancy, and **c** Au absorbed in S divacancy. The Fermi level is set as 0 eV. The COHP algorithm projects the DOS of the material to individual bonds and partitions it into bonding, nonbonding, and antibonding contributions, and the presence of more antibonding states at the Fermi level is considered destabilizing.[4] While the popped S atom causes minuscule (not properly visible in the Fig.) antibonding states (states on the left) at the Fermi level, the Au absorbed at S monovacancy, and divacancy generate massive to moderate antibonding states at the Fermi energy, establishing destabilizing nature of the Au adsorbed configurations compared to the S popped configuration. Also, the integrated value of the COHP (ICOHP) up to the Fermi level, which provides an estimate of bond strengths, is quite high in the case of S popping compared to the other two arrangements. The COHP (-pCOHP) values shown here are calculated as the average value of the COHP values of all the bonds between the atom in question (popped S/absorbed Au) and every atom in its 5 Å radius.

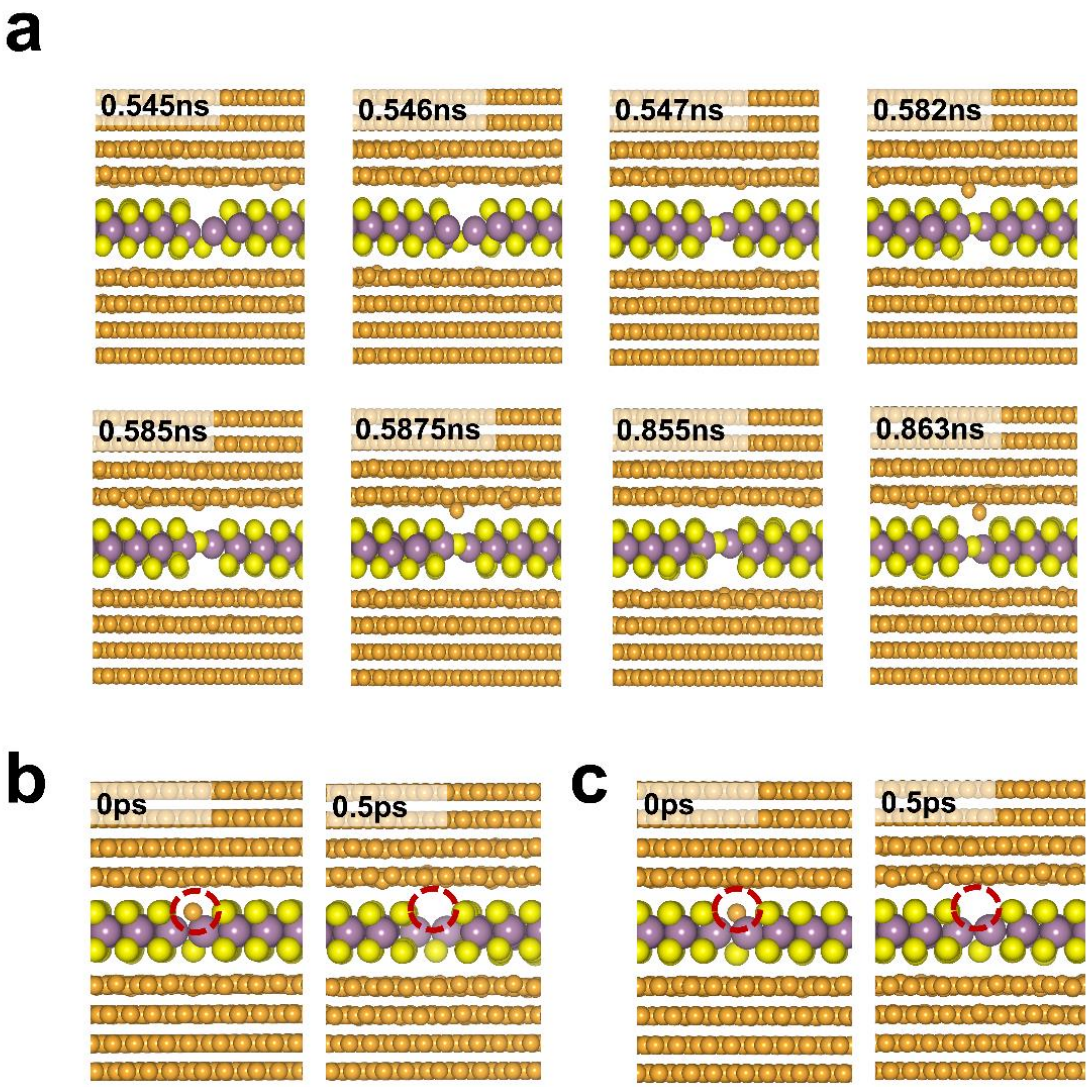

Supplementary Figure 13. Atomistic snapshots of MD simulations on Au-MoS_2-Au system. **a** Zoomed-in side-view images at different time frames under an electric field of 2.75 $VÅ^{-1}$ applied from the top to the bottom electrode. After popping, one Au atom near the popped atoms starts oscillating between the gold and sulfur plane. Snapshots of MD simulations during heating from 30 K to 300 K with **b** a positively charged (+1) and **c** neutral Au atoms manually placed at vacancy locations. The vacancy sites where Au atoms are placed are marked with red circles.

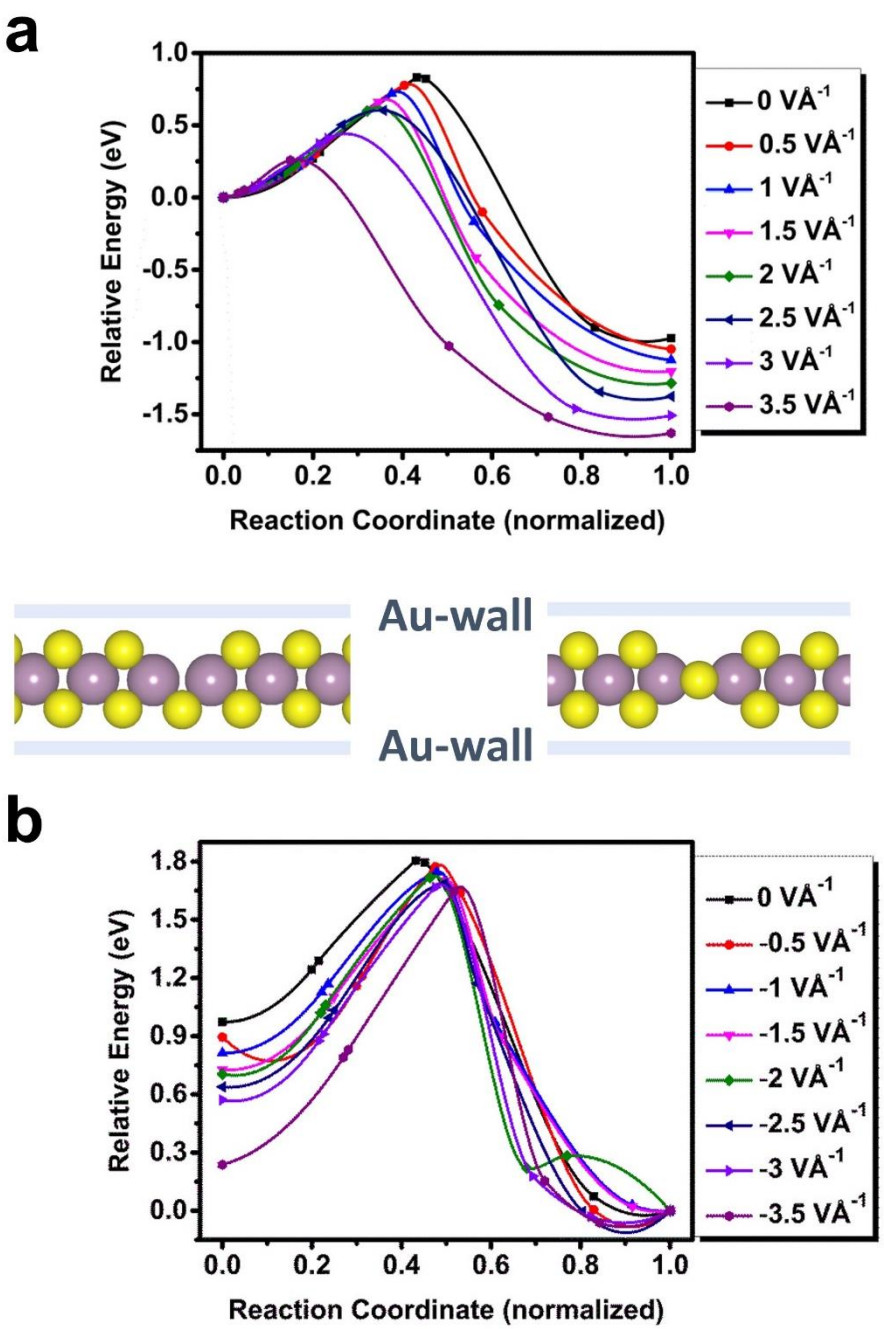

Supplementary Figure 14. CINEB calculations between S vacancy and popped state in MoS_2 monolayer placed between two implicit Au walls. Electric field-dependent activation energy barriers for **a** S atom popping (forward reaction) and **b** return (reverse reaction) in MoS_2 monolayer placed between two implicit Au walls. In the Au walls-based system, the forward barrier is 0.83 eV, and the reverse barrier is about 1.8 eV. Compared to implicit C walls, the forward barrier height is lower in Au walls-based system, implying a lower field is required for popping.

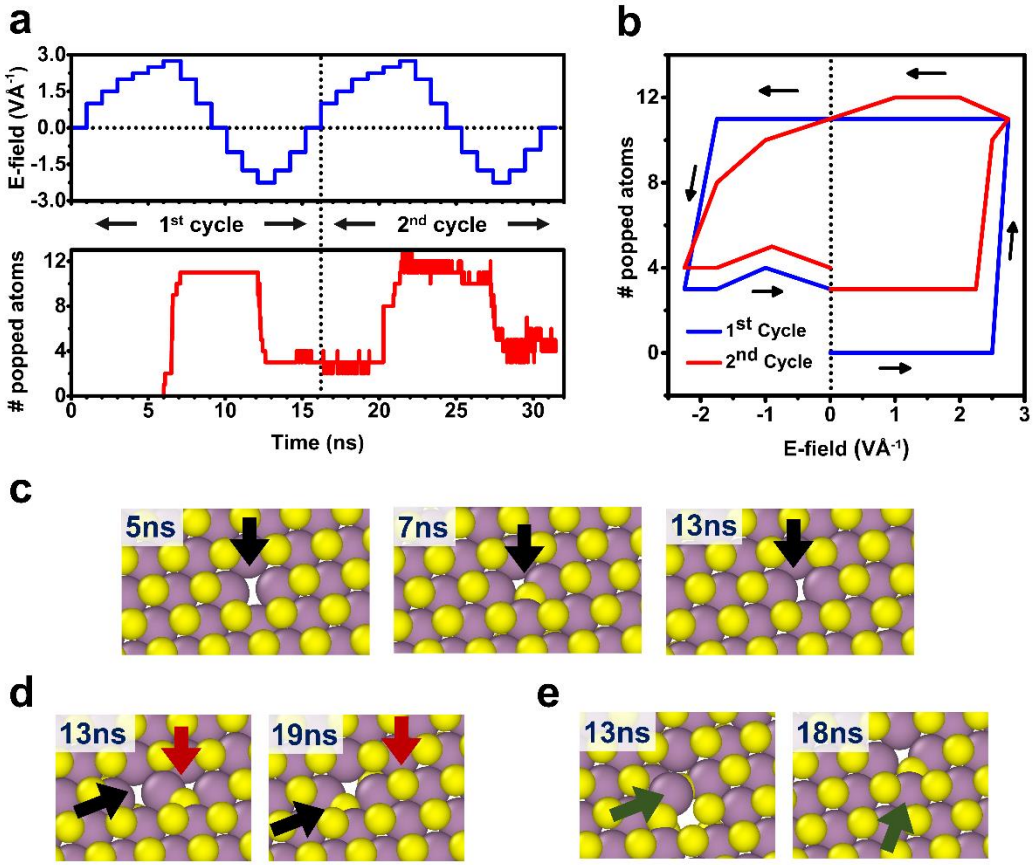

Supplementary Figure 15. Bipolar switching characteristics of Au(wall)-MoS_2-Au(wall) system comprising 12 S monovacancies in one plane. **a** Plot of applied electric field and no. of popped atoms vs. simulation time. **b** Hysteresis plot showing the change in popped atom count with the applied field. The order of application of the field is 0→2.75→0→-2.25→0. Atomistic snapshots zooming-in at the vacancy locations at different points of time displaying different events, **c** initial vacancy location (5ns), S atom popping after set (7ns), popped atom returning after reset (13ns), **d** secondary popping (13ns) during reset and its recovery (19ns) in the next cycle, **e** localized distortion during reset (13ns) and its recovery (18ns). Black, red, and green arrows highlight the vacancy locations, secondary popped atoms, and distorted locations.

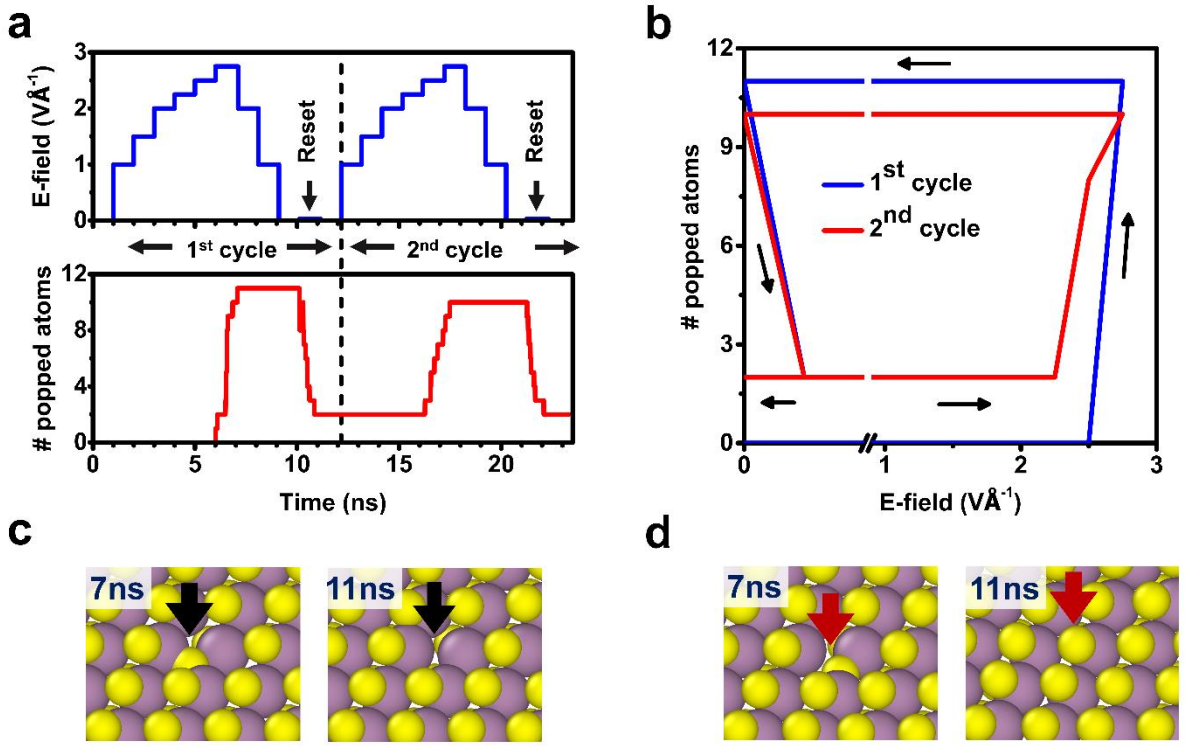

Supplementary Figure 16. Unipolar switching characteristics of Au(wall)-MoS_2-Au(wall) system consisting of 12 S monovacancies. **a** Plot of the applied electric field, and no. of popped atoms vs. simulation time. **b** Hysteresis plot showing the change in popped atom count with the applied field. The order of application of the field is 0→2.75→0→0.025→0. At reset, local temperature around the popped atoms is increased to 1200 K. Atomistic snapshots zooming-in at the vacancy locations displaying **c** S atom popping during set (7ns) and return of the popped atom to its initial location after reset (11ns), **d** S atom popping (7ns) and moving to the opposite plane (11ns).

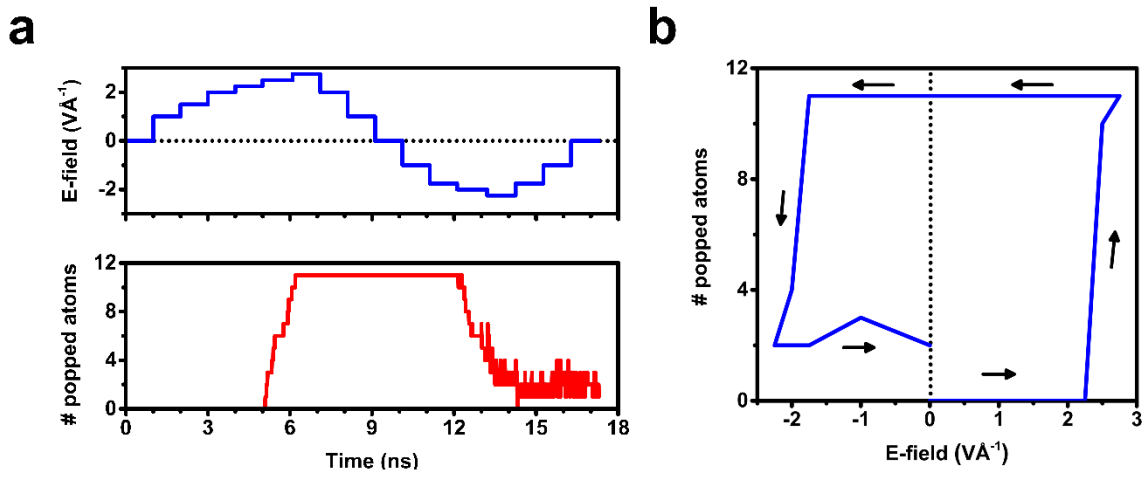

Supplementary Figure 17. Bipolar switching in Au(wall)-MoS_2-Au(wall) consisting of 18 sulfur monovacancies in both S plane (12 in bottom S plane and 6 in top S plane). **a** The plot of applied electric field and number of popped atoms vs. simulation time. **b** Hysteresis plot showing the change in the pop count with the applied field. Theoretically, the S atoms located immediately below the vacancies of the top S plane can be popped up by applying a suitable field in the reverse direction. The applied reverse field of -2.25 VÅ^{-1} is not adequate to pop up those atoms. Only a single atom below the top vacancy gets popped during the reset cycle. However, due to the high local temperature, it returns to its initial location soon. Hence the vacancies in the top S plane do not play any significant role in bipolar switching. But due to the presence of monovacancies in both S planes, unipolar devices can also function with the opposite bias.

Supplementary Note 1

For the implicit Au wall-based system, the distance of walls from the MoS_2 surface is 3 Å. The energy of the wall-MoS_2 interaction is described using Lennard-Jones 9-3 potential. The employed energy and distance parameters in the potential are $\varepsilon = 0.3$ eV, $\sigma = 3.5$ Å, $r_c = 10.0$ Å. These potential parameters are determined by performing a fitting procedure to the plot [Supplementary Fig. 4c] of binding energy vs. interlayer spacing between MoS_2 and Au. The potential energy minimum is found at the interlayer spacing of 3 Å, with a corresponding binding energy of -0.32 eV which is very close to the reported data.[5] In the bipolar switching process, out of 12 vacancies, 11 S atoms pop into the Mo plane as the positive field is increased to 2.75 VÅ^{-1}. At a reverse field of -2.25 VÅ^{-1} with a corresponding local temperature rise to 1200K, the popped atoms return to their initial locations. The local temperature change in set

and reset cycle is shown in Supplementary Fig. 5c, 5d. Similar to the C walls-based system, the secondary pops and local distortion also occur during reset. These anomalous events are completely reversed when a forward field is applied in the 2nd cycle. The variation in voltage and pop count with simulation time, hysteresis loop, and atomic snapshots related to the bipolar switching process of the Au wall-MoS_2 system are shown in Supplementary Figure 6. The bipolar switching of Au wall-MoS_2 system with higher vacancy concentrations (24 vacancies) and monovacancies in both the S planes are also calculated and plotted in Supplementary Figures 11c, d, and 12, respectively. The unipolar switching process is depicted in Supplementary Figure 7. For reset in unipolar switching, a very small positive field of 0.025 $VÅ^{-1}$ is applied, and the local temperature is raised to 1200K. After reset, 90% of the popped atoms return to their initial locations.

In the case of Au explicit electrodes, four layers of [111] surface cleaved bulk Au is added on the top and bottom of the MoS_2 flake. The outer two layers on both sides are fixed during the MD simulation to emulate bulk behavior. Because of the unavailability of reactive force fields, the interatomic forces between Au-Mo, Au-S, and Au-Au atoms are described using Coulomb-corrected LJ 12-6 potential.[6,7] The charges assigned to the Au atoms have been obtained from DFT-based Bader/DDEC analysis. Here also, two distinct Au-MoS_2 interfaces are formed with mean strains of about 2.23% and 0.38%. Again, the electric field is applied to the two innermost MoS_2-adjacent Au layers on each side in addition to the material itself. A similar effect of interfacial strain on the threshold value of the field is observed here. For the higher strain case, the popping event starts at 2.75 $VÅ^{-1}$ whereas, a much higher field (about 4 $VÅ^{-1}$) is required to pop atoms for lower strain. In Supplementary Fig. 14a, the snapshots of pop events in the Au-MoS_2-Au system at different time frames are depicted. After sulfur popping, the Au atom nearest to the popped atom keeps oscillating between the S and Au plane during the entire simulation time frame. Such movement is probably due to the soft attractive, and repulsive nonbonding interaction between the Au and S atoms. However, we do not observe any significant movement of Au atoms before S popping, even with the electric field of both polarities applied to the system.

At the S vacancy sites, we have manually placed both a positively charged (+1e) (Supplementary Fig. 14b) and neutral (Supplementary Fig 14c) Au atom dissociated from the electrode nearest to the vacancy locations and have run MD simulations. LJ potential is unable to define chemical bonds formed between Au atoms with the neighboring Mo and S atoms at the vacancy sites. As soon as the simulation begins, the Au atoms move back to their original

location at the electrode, even if a high forward electric field is applied. It seems without proper reactive potentials, it is challenging to exhibit Au absorption and desorption mechanisms at vacancy sites with the application of suitable forward and reverse bias.

References

1. Bhattacharjee, S. *et al.* Insights into Multilevel Resistive Switching in Monolayer MoS_2. *ACS Appl. Mater. Interfaces* **12**, 6022–6029 (2020).
2. Wu, X., Ge, R., Akinwande, D. & Lee, J. C. Understanding of Multiple Resistance States by Current Sweeping in MoS_2-based Non-volatile Memory Devices. *Nanotechnology* **31**, 465206 (2020).
3. Ge, R. *et al.* Atomristors: Memory Effect in Atomically-thin Sheets and Record RF Switches. in *2018 IEEE International Electron Devices Meeting (IEDM)* 22.6.1-22.6.4 (2018).
4. Rao, F. *et al.* Reducing the stochasticity of crystal nucleation to enable subnanosecond memory writing. *Science* **358** (6369), 1423 (2017).
5. Farmanbar, M. & Brocks, G. First-principles study of van der Waals interactions and lattice mismatch at MoS_2/metal interfaces. *Phys. Rev. B* **93**, 85304 (2016).
6. Trillitzsch, F. *et al.* Directional and angular locking in the driven motion of Au islands on MoS_2. *Phys. Rev. B* **98**, 165417 (2018).
7. Ding, S., Tian, Y., Jiang, Z. & He, X. Molecular dynamics simulation of joining process of Ag-Au nanowires and mechanical properties of the hybrid nanojoint. *AIP Adv.* **5**, 57120 (2015).